Earth Planet. Sci. Lett. 626 (2024) 118530

Contents lists available at ScienceDirect

Earth and Planetary Science Letters

journal homepage: www.elsevier.com/locate/epsl

Evolution in unrest processes at Campi Flegrei caldera as inferred from local seismicity

Stefania Danesi [a], Nicola Alessandro Pino [b,*], Stefano Carlino [b], Christopher R.J. Kilburn [c]

[a] Istituto Nazionale di Geofisica e Vulcanologia, Sezione di Bologna, Bologna, Italy
[b] Istituto Nazionale di Geofisica e Vulcanologia, Sezione di Napoli, Napoli, Italy
[c] UCL Hazard Centre, Department of Earth Sciences, University College London, London, UK

ARTICLE INFO

Editor: Dr C. M. Petrone

Keywords:
Campi Flegrei caldera (CFc)
Volcanic unrest
Hydrothermal system
Seismicity
Fluid circulation
Brittle/ductile transition

ABSTRACT

Changes in seismicity with time and location are diagnostic signals for understanding the dynamics of volcanic unrest. We used these signals at the Campi Flegrei caldera, in southern Italy, to investigate how structural changes have determined three styles of unrest since 1982, distinguished by a ground uplift (measured at Pozzuoli, near the centre of the caldera) of 178 cm in 1982–84; a subsidence of 93 cm in 1985–2005; and an uplift of 118 cm between 2005 and November 2023. Double-difference seismic locations and concentrations of seismic energy release have revealed impermeable horizons that correspond to the cap rock and self-sealed base of the geothermal system at depths of 1.5 and 3 km, respectively. Most earthquakes have been shallower than 3 km, consistent with the brittle upper crust being stretched over a zone of pressurization below the geothermal system. The 1982–84 uplift decayed after a major seismic swarm on April 1st, 1984, breached the lower impermeable horizon, which increased the flux of escaping gas and reduced the source pressure. Continued gas escape promoted subsidence until the lower horizon had resealed itself and initiated a new episode of uplift while gas from depth re-accumulated beneath. Compared with 1982–84, a greater proportion of recent seismicity has occurred at shallower depths below the actively degassing fumaroles of Solfatara-Pisciarelli, north-east of Pozzuoli. The associated high seismic *b*-values, between 1 and 2, are consistent with high fluid pressures and, hence, with locations more favourable to fracturing. Continued uplift may thus persist until fracturing of the shallow crust allows faster rates of gas release and depressurization of the pressure source.

1. Introduction

Campi Flegrei is the largest active caldera in Europe (~12 km diameter) with a population of more than 360,000 people. From the suburbs of Naples, it extends westward to the Tyrrhenian Sea and is partially submerged below the Pozzuoli Bay (Fig 1A). Since pre-Roman times, the Campi Flegrei caldera (CFc) has shown a background trend of slow subsidence occurring at a rate of about 1–2 cm/yr, interrupted by episodes of faster ground uplift (Dvorak and Mastrolorenzo, 1991; Bellucci et al., 2006; Di Vito et al., 2016; De Vivo et al., 2020) accompanied by widespread occurrences of volcano-tectonic (VT) seismicity (Corrado et al., 1977; Del Pezzo et al., 1987; Petrosino et al., 2008). Since 1950 four episodes of caldera-wide ground deformation have raised the coastal town of Pozzuoli, located near the centre of largest uplift, by more than 4 m (Fig. 1B; Del Gaudio et al., 2010). The first three episodes interrupted the secular subsidence of the caldera with comparable amounts of uplift in both duration and amplitude: about 74 cm in 1950–52, 159 cm in 1970–72, and 178 cm in 1982–84 (Fig. 1B; Del Gaudio et al., 2010). Scarce seismic activity was observed during the 1970–1972 unrest. In contrast, the seismic stations of the Osservatorio Vesuviano (OV) recorded more than 16,000 shallow VT earthquakes (with maximum magnitude $M_d = 4.0$) during the 1982–84 crisis (OV; Del Pezzo et al., 1987; Petrosino et al., 2008), coinciding with an uplift at Pozzuoli of about 178 cm between June-July 1982 and the end of December 1984 (Dvorak and Berrino, 1991; Del Gaudio et al., 2010; De Martino et al., 2021). Subsidence began shortly after and continued for c. 20 years, lowering Pozzuoli by 93 cm, at an average rate 2.6 times faster than secular subsidence. Unrest returned in 2005 with the lowest rate of uplift in the last century (c. 5 cm/year; Figs 1B and 1C). By April 2022, the uplift had recovered the previous two decades of subsidence (INGV, 2023). Persistent seismicity returned in 2012–14, since when the mean rate has continued to increase (Fig. 1C) and, by February 2023,

* Corresponding author.
E-mail address: alessandro.pino@ingv.it (N.A. Pino).

https://doi.org/10.1016/j.epsl.2023.118530
Received 28 July 2023; Received in revised form 26 November 2023; Accepted 2 December 2023
Available online 13 December 2023

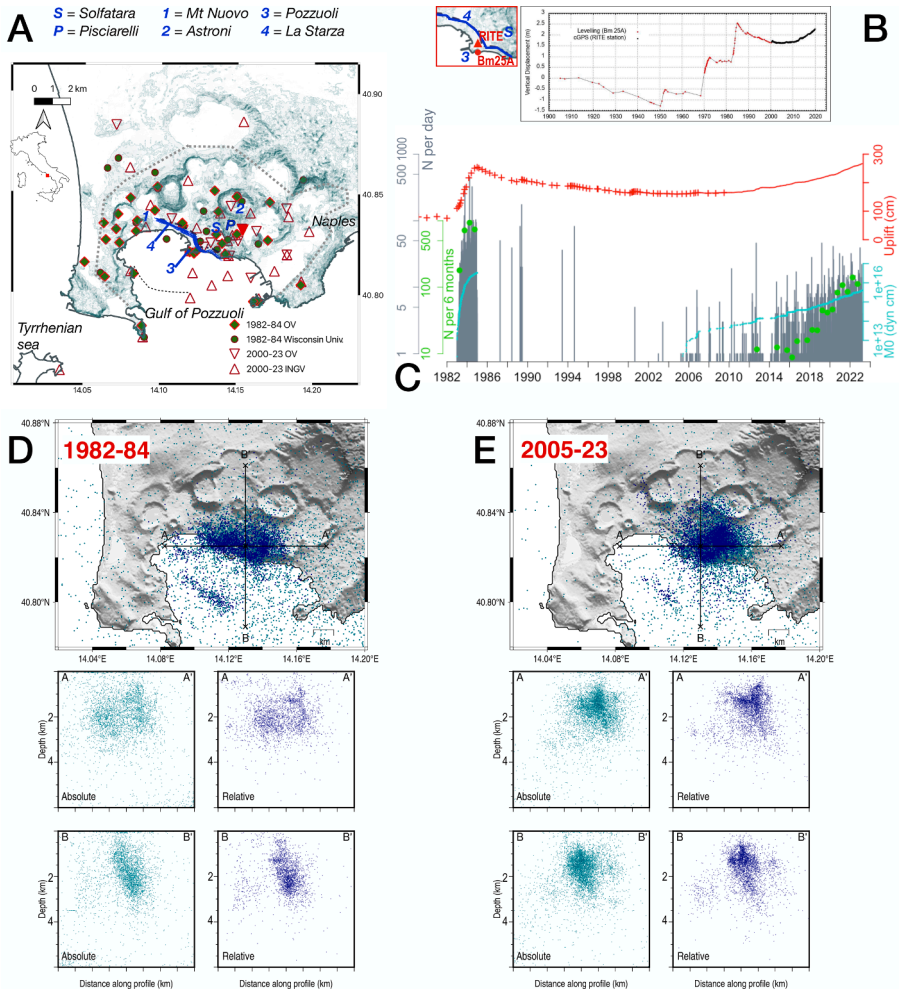

Fig. 1. (A) Map of the Campi Flegrei area and geometry of the seismic monitoring networks in 1982–84 (squares managed by INGV-Naples (OV); circles managed by the University of Wisconsin), and after 2000 (triangles managed by INGV-Rome and upside-down triangles managed by INGV-Naples). Station STH is shown by the solid red triangle. The dotted gray line follows the inner edge of CFc (Natale et al., 2022). The dashed line offshore represents a segment of the inner edge of the caldera (Natale et al., 2022). 1 = Monte Nuovo, 2 = Astroni crater, 3 = Pozzuoli, 4 = La Starza marine terrace, *S* = Solfatara fumarole, *P* = Pisciarelli fumarole. (B) Vertical displacement at CFc from 1905 to December 2019 (De Martino et al., 2021). Red dots are levelling data at benchmark Bm25A, black dots are GPS measurements at Station RITE. Both sites (Bm25A and RITE) are in Pozzuoli (inset) (C) The gray bars are the number of VT seismic events per day for 1982–2023 (gray logarithmic scale). The green dots are the cumulative number of VT events per 6 months (logarithmic scale). The cyan dots are the cumulative seismic moment M0, calculated with the method of Petrosino et al. (2008); secondary axes). The vertical displacement for 1982–2023 is referenced to 1905: red crosses are high-precision levelling measurements at benchmark Bm25A; red points are GPS measures at RITE station. (D) Map and vertical sections of the distribution of absolute (green) and relative (blue) seismic locations for the 1982–84 unrest. Vertical sections are cut along the two perpendicular transects AA' and BB' in map. (E) As for (D), but in 2005–23. The magnitudes of completeness are 0.5 for 1982–84 and 0.2 for 2005–23.

more than 7000 events had been detected (INGV, 2023).

The VT events at CFc have occurred at depths of about 3 km or less, within crust that hosts a high-temperature hydrothermal system (temperature gradients in deep boreholes exceed 150 °C/km to depths of 3 km), the base of which appears to correspond to the brittle-ductile transition zone (BDTZ) (Carlino, 2018; Castaldo et al., 2019). VT events can be triggered by several processes, including changes in the stress field of the host rocks, directly induced by the uplift and migration of magma or magmatic fluids (Suzuki, 1959; White and McCausland, 2016); the tendency to increase fracture density in highly heterogeneous materials (Mogi, 1962); thermal stress, particularly in the presence of hot fluids causing high thermal gradients (Warren and Latham, 1970). At the CFc, the VT seismicity and ground movement have been driven by changes in the volcanic-magmatic system, rather than the regional stress across the caldera (Rivalta et al., 2019). Specific controls have been linked to spatial and temporal variations in the stress field associated with volcanic dynamics (Dvorak and Berrino, 1991; Macedonio et al., 2014; D'Auria et al., 2015) or to fluid circulation within the hydrothermal system (Di Luccio et al., 2015; Chiodini et al., 2021; Petrosino and De Siena, 2021). In addition to VT events, long-period (LP) earthquakes are rarely recorded in the CFc, mainly due to perturbations in the shallow pressure field that induce resonance in fluid-generated fractures (Cusano et al., 2008).

The unrest episodes have been caused by pressure changes in fluids below the BDTZ at depths of c. 3–4 km (Dvorak and Berrino, 1991; Gottsmann et al., 2006a, 2006b; Woo and Kilburn, 2010; D'Auria et al., 2011; Troise et al., 2019) which, in turn, may have disrupted the circulation of fluids within the overlying hydrothermal system and reinforced the total amount of surface deformation and VT seismicity (Di Luccio et al., 2015; Tamburello et al., 2019; Chiodini et al., 2021; Petrosino and De Siena, 2021; Lima et al., 2021; Todesco, 2021; Bonafede et al., 2022; Buono et al., 2022).

The fluids available below the BDTZ are magma or magmatic gas, notably CO_2 (Buono et al., 2022). The sources for both are a melt-rich zone about 7–9 km below the surface (Tamburello et al., 2019; Chiodini et al., 2021; Buono et al., 2022).

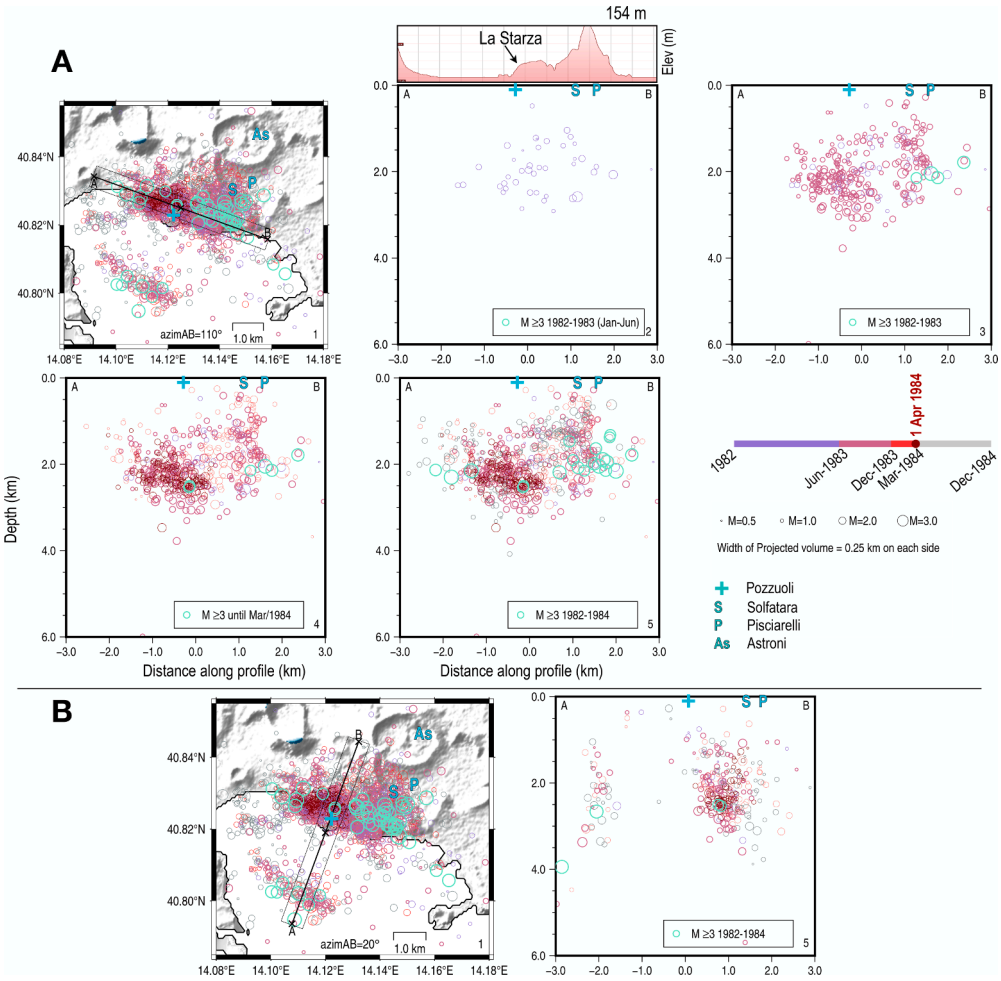

Fig. 2. (A) Relative seismic locations for the 1982–84 time-window, in map (Panel 1) and vertical profile AB over time (Panels 2–5). Profile AB is oriented 110°N and 6 km long. The projected volume is 0.5 km wide. Circle size is proportional to magnitude (legend), colours change as a function of time (note the 1st Apr 1984 swarm in dark red); green circles; indicate events with $M \geq 3$. The topographic elevation (in m) along the profile AB is plotted above the Panel 2 (elevations from Google Earth Pro). Pozzuoli, Astroni, Solfatara and Pisciarelli are marked in cyan. The catalog has been truncated for a completeness magnitude Mc = 0.5. (B) Map and vertical section for a perpendicular 20°N-oriented profile. Colours as for (A).

The gas is dominated by CO_2 (Caliro et al., 2007; 2014; Chiodini et al., 2021) which, during the first half of 2023, had an average flux of c. 4000 tonnes/day from the Solfatara-Pisciarelli fumaroles, c. 2–2.5 km NE of Pozzuoli harbour (INGV, 2023). Although 20–40 % may be non-magmatic (caused by decarbonation of hydrothermal calcite; Buono et al. (2023)), the magmatic component remains comparable to fluxes at active volcanoes with sustained outgassing (INGV, 2023).

The evolving behaviour during successive episodes of unrest (with variations in ground deformation, seismicity rate and geochemical parameters) is consistent with a single, long-term sequence of crustal extension (Kilburn et al., 2017; 2023). The dominant fluid being pressurized beneath the BDTZ may also have changed between episodes from magma during the short, rapid uplifts before 1984 to magmatic gas during the slow, long uplift since 2004 (Kilburn et al., 2023). Here, we compare the patterns of VT seismicity during the current (since 2005) and previous (1982–84) episodes of unrest to identify new constraints on structural changes in the crust and the evolution of the ongoing unrest. Our results show that the caldera's behaviour since 1982 is consistent with a single, long-term response to pressurization in 1982–84 breaching impermeable horizons beneath the geothermal system and disrupting the flow of magmatic gas through the upper crust. They also suggest that continued unrest will favour more extensive fracturing and gas release, with outcomes ranging from a deceleration in ground movement to phreatic explosions and, in the extreme, to conditions suitable for renewed magma ascent from depth.

2. Data and methods

To examine the seismic characteristics of CFc's unrest, we first derived the relative locations, rates of energy release and magnitude-frequency relations for earthquakes since 1982.

2.1. Double-difference earthquake location

The 1982–84 unrest was monitored by a local network of vertical-component, short-period, analog seismic stations (Fig. 1A), with estimated magnitude of completeness $M_c = 0.5$ (Scarpa et al., 2022). It was supplemented between August 1983 and May 1984 by a temporary three-component, short-period, digital network from the University of Wisconsin (Aster and Meyer, 1988). Since the early 2000s, the network has been significantly modernised and its performance has improved (Bianco et al., 2022). At the time of writing, the seismic network consists of 26 broad-band 3-component digital stations, with real-time data transmission (Fig. 1A). The completeness magnitude for the network is 0.2 (Tramelli et al., 2021).

Seismicity was almost absent during the subsidence between 1985 and 2005; it occurred only in a very restricted area around Solfatara, in the form of short-lived swarms (one or a few days) spaced months or

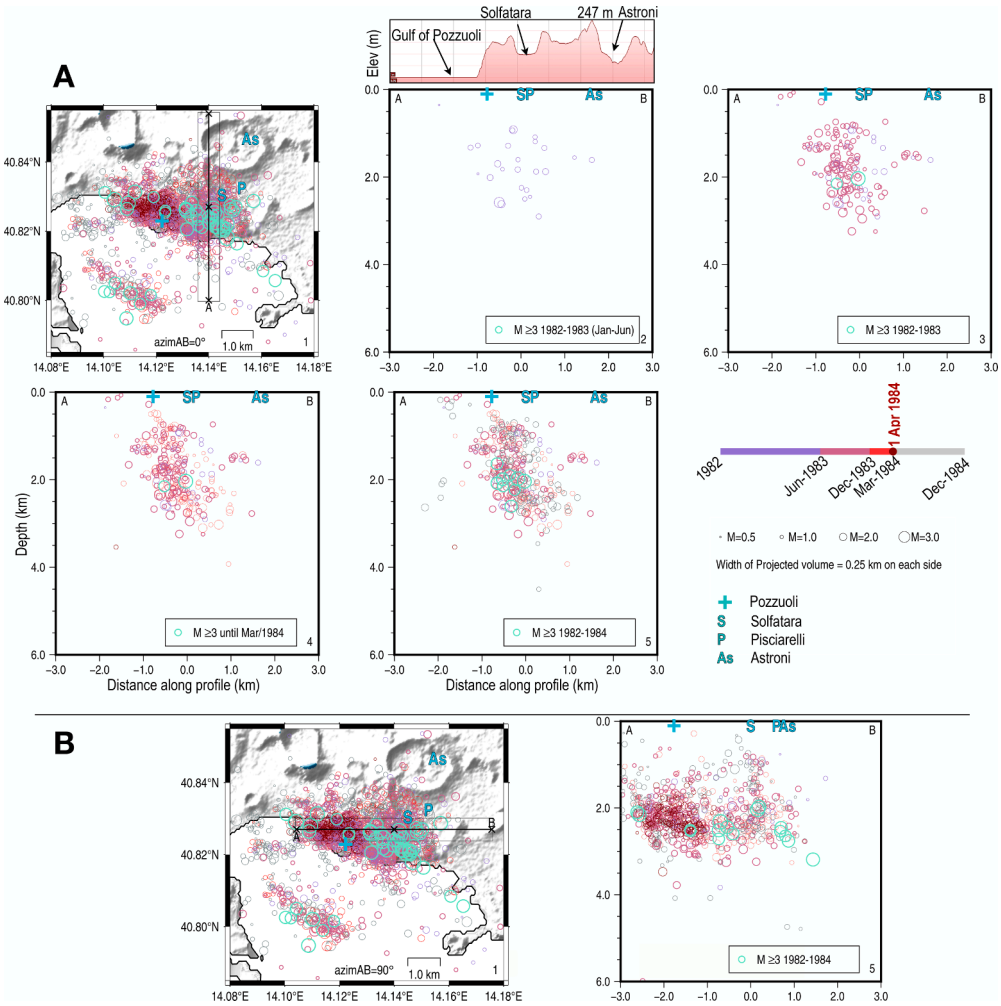

Fig. 3. (A) Relative locations for the 1982–84 earthquakes in map (Panel 1) and vertical profile AB (Panels 2–5). Profile AB is NS-oriented, 6 km long, and centred on Solfatara. The projected volume is 0.5 km wide. Circle size is proportional to magnitude (legend), colours change as a function of time (note the 1st Apr 1984 swarm in dark red); green circles indicate events with $M \geq 3$. The topographic elevation (in m) along the profile AB is plotted above the Panel 2 (elevations from Google Earth Pro). Pozzuoli, Astroni, Solfatara and Pisciarelli are marked in cyan. The catalog has been truncated for a completeness magnitude Mc = 0.5. (B) Map and vertical section for a perpendicular EW-oriented profile. Colours as for (A).

years apart. (Fig. 1C; Orsi et al., 1999; D'Auria et al., 2011; Global Volcanism Program, 1989). For this reason we neglected the 1984–2004 interval, and focused instead on the seismicity of the unrest 1982–84 and 2005–23. Time series for the daily number of earthquakes show that swarm activity superimposed on more continuous seismic activity during both intervals (Fig. 1C; Supplementary Materials).

For the two time intervals 1982–84 and 2005–23, we analysed the differential P and S arrival times for pairs of events extracted from the manually revised INGV-Naples database to perform a relative double-difference location with the HypoDD algorithm (Waldhauser, 2001). Arrival times at stations operating in both periods were included. We examined the two seismic datasets separately to account for disparities in the monitoring system, while maintaining the same inversion scheme. We first performed the absolute location for all events with the Hypoinverse algorithm (Klein, 2002) using station delay time when known, distance weighting for P and S arrival times, and an *ad-hoc* calibrated 1D reference seismic velocity model (Table 1S Supplementary Materials). Based on the differential travel times of the event pairs, the pre-processing of the double-difference inversion selected 8142 and 5037 linked events, respectively for the years 1982–84 and 2005–23 (Fig. 1D and Fig. 1E, green dots). The inversion procedure required: three sets of iterations; the use of the Least SQuaRe (LSQR) algorithm which is suitable for large datasets; at least 8 observations per pair of events; weighted P and S arrival times; a maximum distance of 2 km between linked events; and a damping parameter equal to 200.

2.2. Seismic energy release

We estimated the cumulative square root of the seismic energy release as a proxy for co-seismic strain release (Benioff, 1951). We used the duration magnitude M_d, which is the measure of earthquake magnitude that INGV in Naples routinely estimates and officially communicates to the National Civil Protection in the INGV Seismic Bulletins (INGV, 2023). This measure is preferred to account for the large percentage of micro-seismicity ($M_d < 1$) and to maintain homogeneity with catalogues from 1982 onward. It is manually calculated from the waveform coda at a short-period seismic station (STH, in Fig. 1A). We derived the moment magnitude (M_w) from catalogues of M_d for the two periods of unrest (Ricciolino and Lo Bascio, 2021; Tramelli, 2022), by applying the empirical magnitude-duration relation of Orsi et al. (1999) and calibration laws for magnitude scales from Petrosino et al. (2008). To estimate the cumulative seismic energy distribution E_s, we divided the seismogenic volume into a regular grid with nodes 0.2 km apart and applied the energy-magnitude relationship of Kanamori (1977): $\log E_s = 11.8 + 1.5 M_W$.

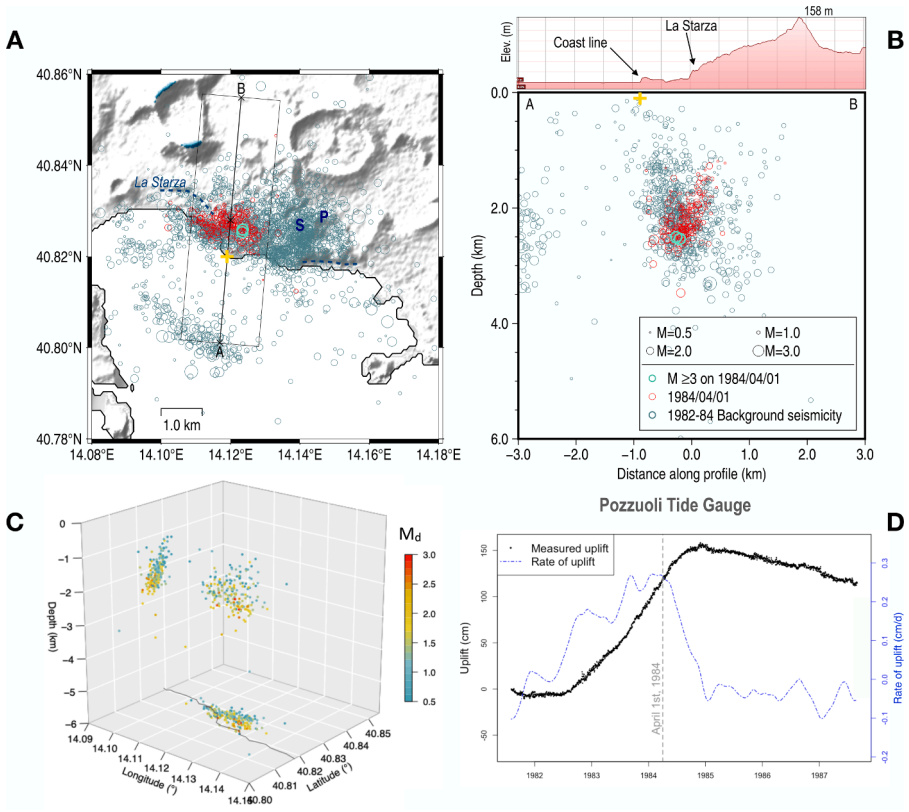

Fig. 4. (A) The relative locations for the 1st April 1984 swarm (red circles) superimposed on the background seismicity for the entire period 1982–84 (teal circles). The size of circles is proportional to the magnitude (legend in B). The green circles show the two $M_d = 3$ earthquakes. AB is the 6-km long profile, 10°N-oriented, used for the vertical section, and the box indicates the perimeter of the projected volume (1.5 km wide). (B) Vertical section along the profile AB (symbols as in (A)). The topographic elevation (in m, from Google Earth Pro) along the profile AB is plotted above the vertical section. (C) 3D representation of the swarm: absolute and relative locations are projected onto horizontal and vertical sections. The colour code changes with magnitude following the scale. The coast line is in black on the bottom plan. (D) Black points represent the daily measure of the ground displacement acquired by the tide gauge of Pozzuoli between 1982 and 1984 (primary axis; Berrino, 1994). The blue dash-dotted line is the smoothed rate of uplift in cm per day (secondary axis).

2.3. Gutenberg-Richter b-value and stress patterns

We calculated the seismic *b*-value (Gutenberg and Richter, 1955) to investigate variations in the size distribution of earthquakes and its relation to changes in local stress. For the size distribution, we used the relative earthquake locations on a regular grid with 0.05 km spacing. Each estimate was based on at least 150 events, of which at least 50 with duration magnitudes above the completeness value M_c within 0.5 km from each grid node; M_c was obtained by the maximum curvature technique (Wiemer and Wyss, 2000). To investigate changes in local stress after seismic swarms, we calculated changes in *b*-value for VT events in a cylindrical volume centered on Solfatara and, with a radius of 0.7 km, large enough to include a representative proportion of swarms (Supplementary Materials, Table S2).

3. Results

3.1. Relative locations of earthquakes

As shown in Fig. 1D and 1E, the HypoDD inversion returned the relative location for 3062 events in 1982–84 (time residuals of 0.05–0.4 s with a median of 0.9 s) and of 3355 events in 2005–23 (time residuals of 0.01–0.09 s with a median of 0.04 s). The median spatial errors for the three components are in the range 77–100 m for 1982–84 and 31–40 m for 2005–23.

3.2. Evolution of seismicity patterns over time

3.2.1. 1982–1984

Figs. 2 and 3 show the time evolution of the 1982–84 seismicity projected over two sets of orthogonal vertical sections with principal directions NW-SE along the caldera's coastline and N-S across Solfatara. Only sporadic and weak seismicity occurred until the first half of 1983, after which the event rate accelerated significantly (Fig. 2A). The coastline section shows two broad clusters of events: one about 2 km wide at depths of 1.5–3 km below Pozzuoli (Fig. 2A), and another with an oblique, upward alignment between 3 and 0.5 km below Solfatara (Fig. 2A and 3A). Fewer events occurred offshore. In the southwestern part of the Bay of Pozzuoli, they showed a NW-SE alignment (Figs 2B) along a recognized fault structure (Di Luccio et al., 2015; Natale et al., 2022). The sub-horizontal cluster at depths of 1.0–1.5 km between Solfatara and Pozzuoli (Fig. 3A) represents the upper limit for seismicity west of Solfatara throughout the entire unrest. In the NS direction the seismicity did not extend more than 1 km from Solfatara, apart from a small cluster 1.5 km deep on the edge of the Astroni crater and about 2 km north of Solfatara (Fig. 3).

On April 1st, 1984, a swarm of over 500 events (Barberi et al., 1984) occurred beneath Pozzuoli (Figs. 2A and Fig. 3B, dark red circles) at depths between 1 and 3 km; the two largest events with $M_d = 3.0$ occurred at 04:27AM UTC and 04:43AM UTC (Tramelli et al., 2021).

For this swarm, we analysed data from 368 events in the $0.2 \leq M_d \leq 3.0$ magnitude range and obtained 217 relative HypoDD locations with a minimum M_d of 0.4 (Fig. 4). The epicentres closely followed the marine terrace of La Starza (Fig. 4A), while the hypocenters occurred along a

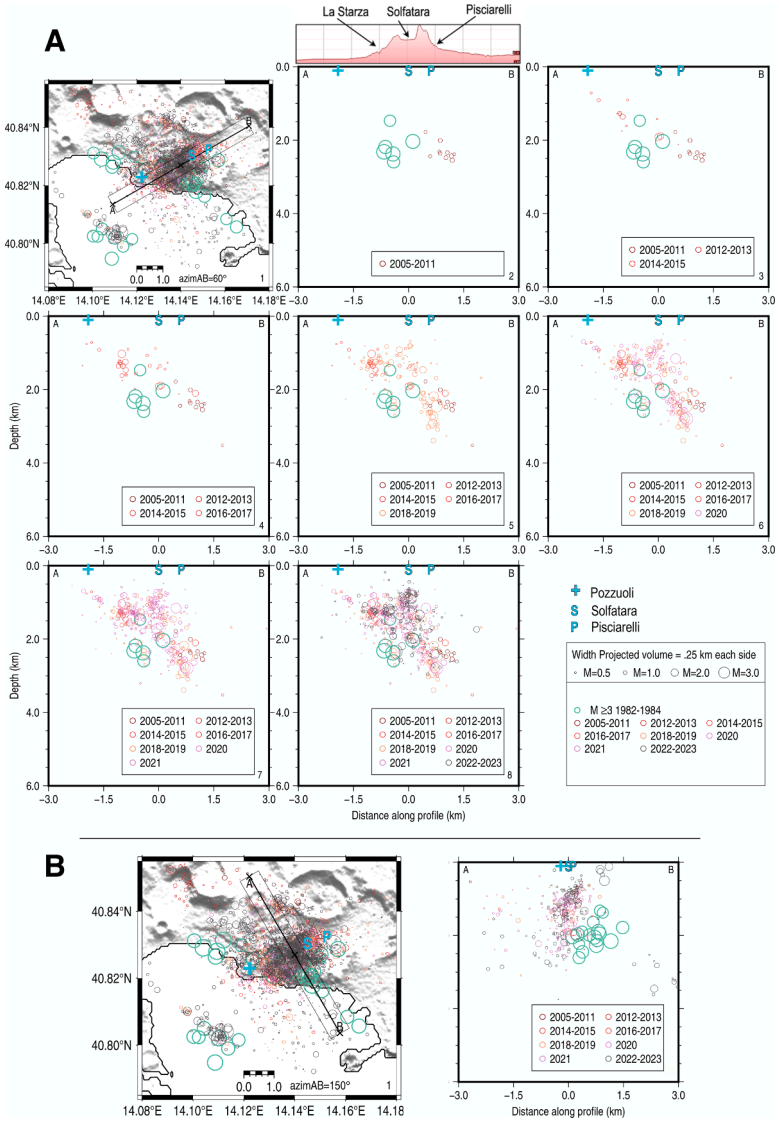

Fig. 5. (A) Relative locations of earthquakes with time for the 2005–23 in map (Panel 1) and vertical section AB (Panels 2–5). Profile AB is 60°N-oriented, 6 km long, and centred on Solfatara. The projected volume is 0.5 km wide. The size of circles is proportional to magnitude (legend). Colours change as a function of time (code on right). The green circles indicate events with $M \geq 3$ during the 1982–84 unrest. The topographic elevation (in m) along the profile AB is plotted above Panel 2 (elevations from Google Earth Pro). Pozzuoli, Solfatara and Pisciarelli are marked in cyan. The catalog has been truncated for a completeness magnitude $M_c = 0.2$. (B) Map and vertical section for a perpendicular 150°N-oriented profile, centred at Solfatara. Colours are the same code as in (A).

well-defined oblique alignment between depths of 1 and 3 km. Larger events tended to occur at greater depths and all those with $M_d \geq 2$ were deeper than 2 km (Fig. 4C). The distributions together indicate the activation of a c. 2 × 2 km^2 structure dipping at high-angle towards the SW (Fig. 4B and 4C). The swarm marked a change in ground movement and the pattern of seismicity. First, the rate of ground uplift began a long-term decay from its peak value of c. 0.2 cm/day until the end of unrest (Fig. 4D). Second, although 1.5 km away from the swarm itself (Fig. 3B), Solfatara became a focus for large-magnitude events: before the swarm, only two events with magnitudes $M_d \geq 3$ had occurred in its vicinity, on 24 November ($M_d = 3.5$) and 30 December 1983 ($M_d = 3.8$; Fig. 3A, green circle); after the swarm, in contrast, locations beneath Solfatara produced most of the high-magnitude events until the end of unrest (more than 30 with $M_d \geq 3$; Fig. 3).

3.2.2. 2005–2023

The 1984 crisis was followed by twenty years of occasional seismicity while the ground subsided by c. 0.9 m (Fig. 1C). Weak seismicity resumed c. 1 km NE of Solfatara when uplift began again in 2004–2005. By February 2023, three spatially distinct clusters could be recognised from the WSW-ENE profile in Fig. 5A:

(i) An oblique alignment deepening from about 2 km beneath Solfatara to c. 3 km about 1.5 km to the northeast.
(ii) A sub-horizontal cluster at depths of 1.0–1.5 km in the hydrothermal system between Solfatara and Pozzuoli. It extends laterally for less than 1.5 km and, with the exception of a very shallow oblique alignment extending towards the coast line, marks the upper limit for seismicity west of Solfatara (Fig. 5A). The extent of this cluster confirms the presence of a fracture-resistant cap rock overtopping the seismogenic volume W of Solfatara, previously identified by Vanorio and Kanitpanyacharoen (2015) and imaged by velocity and attenuation tomography (Calò and Tramelli, 2018; De Siena et al., 2017)
(iii) Since 2018, a shallow cluster (at depths of less than 1 km) appears to have been developing beneath Solfatara in the direction of Pisciarelli to the northeast.

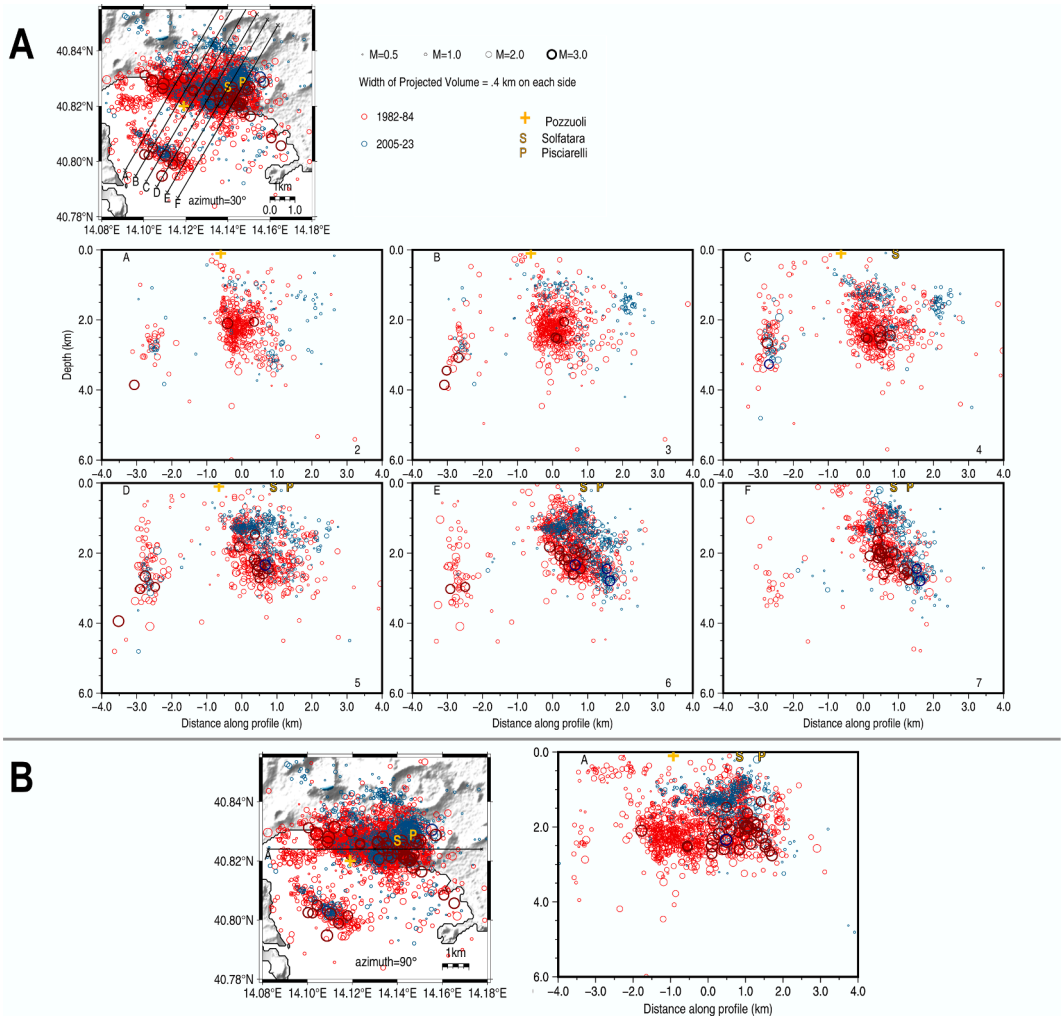

Fig. 6. Relative locations of VT events for 1982–84 (red circles) and 2005–23 (blue circles). Events of magnitude $M \geq 3$ are shown by thick, dark circles. (A) Map of relative locations along six 8 km long profiles oriented at 40°N that cross CFc from SW to NE. Panels A-F show each vertical section. The projected volumes extend 0.25 km on each side of each profile. (B) Map and vertical section for the EW profile. The projected volume extends 0.5 km on each side of the profile. Colours as in (A).

The perpendicular profile (Fig. 5B) highlights the migration of events shallower than 1.5 km towards the southeast, and the lack of significant seismicity more than 1 km from Solfatara and deeper than 1–1.5 km.

3.3. *Comparative distributions of earthquakes in 1982–84 and 2005–23*

Low seismicity has occurred west of Solfatara in 2005–2023. At depths of 1.5–3.0 km between Pozzuoli and Solfatara, only isolated and low-energy events have occurred since 2005, in contrast to the pronounced seismicity in 1982–84 that included duration magnitudes greater than 3. The difference has been accentuated by the cluster of events developing at depths of 2–3 km beneath Solfatara since 2005. This cluster appears to be slightly shifted to the NE compared with 1982–84. Another new feature is the cluster of shallow earthquakes extending from depths of 0.5–1 km toward Pisciarelli; seismicity in this volume was barely evident in 1982–84 (Figs 6A and 6B).

For both periods, low-magnitude seismicity has been distributed between Pozzuoli and Solfatara, at a depth of 1–1.5 km (B-C-D-E), with the density of events increasing towards Solfatara.

In 1982–84 a major offshore structure was active 2–3 km from the coast, oriented NW-SE and about 3 km long. The orientation of the fault structure changes with depth. Thus its mean dip is c. 70° SW (Fig. 6A, Profiles A-C) between 2 and 4 km below the surface, but sub-vertical (possibly dipping steeply to the NE) at shallower levels (Fig. 6A, Profiles D-F). The angles are consistent with previous estimates based on a smaller number of events (Orsi et al., 1999). All the events with $M_d \geq 3$ occurred along the deeper segment (Figs 2B & 6A). After 2005, the segment between 2 and 3.5 km depth of the same structure was activated, with a significant event ($M_d = 3$, reverse mechanism from INGV Bulletin data; INGV, 2023) on 2023/02/05.

3.4. *Energy release*

The total Benioff strain released during the 1982–84 unrest is more than one order of magnitude larger than that released during 2005–23 (Fig. 7). For 1982–84, horizontal (Fig. 4Sb) and vertical sections (Fig. 7) indicate that most of the strain energy was concentrated along a horizontal belt that extended across the caldera, at a depth between 2 and 3 km. Peak values within this horizon were located beneath Solfatara. A smaller concentration can also be seen at depths of c. 1.5 km and below Solfatara (Fig. 7). At depths greater than 3 km, strain tends to have accumulated beneath the outer margins of ground uplift (Fig. 4Sb).

For 2005–23 the strain has instead been focused in small volumes corresponding to the three main clusters of earthquake locations (Section 3.2.2): along the 1–1.5 km horizon between Solfatara and Pozzuoli; about 0.5–1.0 km below Solfatara-Pisciarelli; and in a volume 1 km NE of Solfatara at depths of 2.5–3 km.

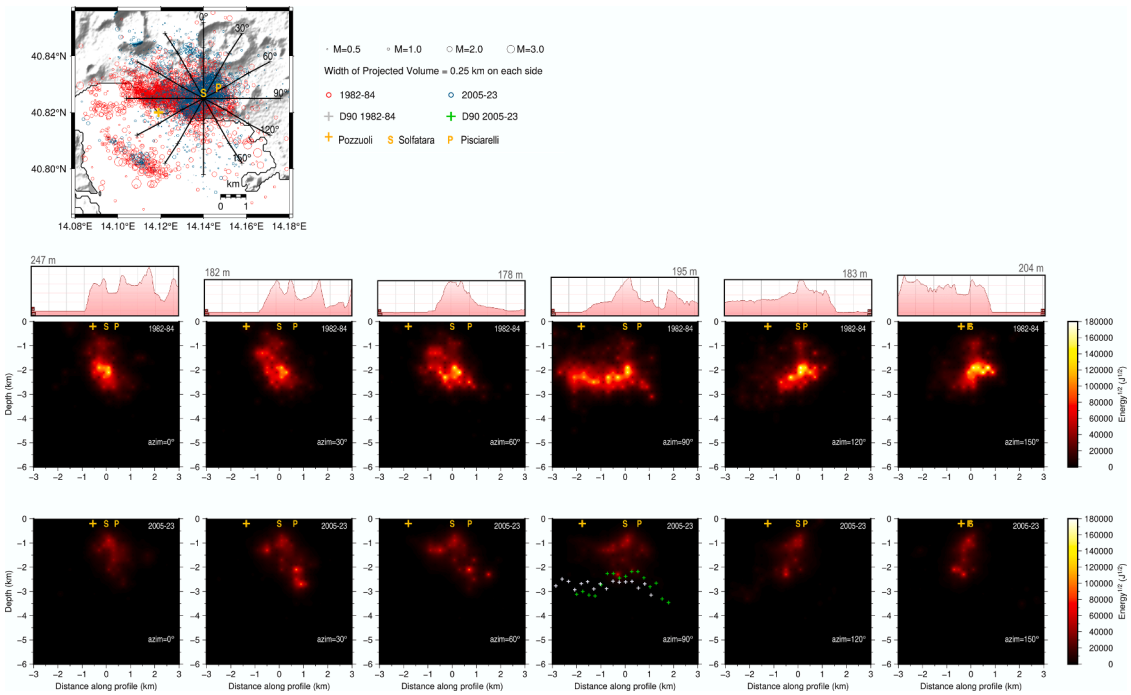

Fig. 7. Map and vertical sections of the Benioff strain for 1982–84 (red points) and 2005–2023 (blue points). The black lines on the map are 6 km long profiles centred on Solfatara and radially spaced at 30° The vertical sections give the square root of the seismic energy released in a 0.5 km wide volume projected onto each profile. Grey and green crosses in the EW oriented vertical section mark the D90 cutoff depth for the two distributions of seismicity 1982–84 and 2005–23, respectively. Pozzuoli, Solfatara and Pisciarelli are marked in yellow.

3.5. *Gutenberg-Richter b-value*

The magnitude-frequency distribution of earthquakes in 1982–84 has a seismic *b*-value of 0.89 ± 0.02 (Fig. 8). Maximum values occurred among earthquakes below Solfatara (depths <1 km) and the position of maximum uplift near Pozzuoli (depth of c. 1–1.5 km and c. 2–3 km). In 2005–23, the *b*-value was 0.92 ± 0.02, with peak values up to 2 ± 0.03, again below Solfatara (depths <0.5 km) and close to the centre of uplift (depths c. 1.0–1.6 km); a small concentration is also apparent about 1.5 km west of Solfatara at a depth of c. 1 km (Fig. 8). Peak values of the *b*-value for the current unrest are generally higher than for the 1982–84 unrest.

Since 2020, the *b*-value has been increasing by about 70–80% beneath Solfatara and Pisciarelli to a depth of 2.5 km, as well as in the 1.5 km horizon west of Solfatara (Fig. 9). Increases in *b*-value beneath Solfatara are roughly related to the occurrence of swarms (Fig. 7S).

4. Discussion

4.1. *Major patterns of seismicity*

Seismicity in 1982–84 and 2005–23 has been dominated by movements across related sets of faults. In 1982–84, almost all earthquakes occurred at depths of less than 3.5–4 km and had epicentres distributed close to the coastline, starting east of Solfatara and crossing the hydrothermal system to the west (Fig. 6). For both periods, most of the largest events have been located at depths of 2–3 km, near the base of a NE-dipping structure that defines the eastern boundary of the seismic zone (Fig. 6). A secondary concentration of epicentres occurs along a NW-SE alignment 2.5 km to the southwest, beneath the Bay of Pozzuoli (Fig. 6).

The limiting depth of c. 3 km for seismicity and strain energy release lies close to the depths of the Brittle-Ductile Transition Zone (Carlino, 2018; Castaldo et al., 2019) and to the locations of pressure sources inferred from patterns of ground deformation (Dvorak and Berrino, 1991; Gottsmann et al., 2006a, 2006b; Woo and Kilburn, 2010; D'Auria et al., 2011; Troise et al., 2019). Apart from the shallow seismicity below Solfatara, few earthquakes have occurred at depths less than 1 km (Fig. 6). This depth approximately coincides with the base of a fracture-resistant cap rock proposed by Vanorio and Kanitpanyacharoen (2015). Such a horizon would promote fluid accumulation in the underlying rock and the onset of fluid-induced fracturing (Akande et al., 2021).

The seismogenic zone of the CFc thus appears to be bounded (1) by two levels where the crust's mechanical properties change significantly (a strong, shallow cap rock and a deeper transition from a brittle to ductile rheology), and (2) by well-established fault systems around its lateral margins. Despite these common features and the similarity in the quasi-radial symmetric pattern of ground deformation (Berrino et al., 1994; De Martino et al., 2021), suggesting a similar source location and overpressure value, the uplift rate (Fig. 1C), the spatial distribution of seismicity (Fig. 6), and the seismic energy release (Fig. 7) show significant differences for the two periods 1982–84 and 2005–23. In particular, for the current unrest, the uplift rate is about 8 times lower than in 1982–84, earthquakes below the point of maximum uplift are substantially absent, while the seismically released energy is one order of magnitude lower than in 1982–84 and mainly located in narrow volumes below Solfatara-Pisciarelli area.

4.2. *Structural changes in the crust since 1982–84*

The base of the seismogenic zone corresponds with the BDTZ inferred from the temperatures and compositions of rocks from deep borehole (e.g. Carlino, 2018 and references therein). Adapting the model of Fournier (1999), we interpret this layer to be a self-sealing horizon that separates deeper crust that can achieve lithostatic pore pressure from overlying crust at hydrostatic pore pressure. Lithostatic pore pressures below the BDTZ are favoured by CO_2 from depth maintaining a gas-saturated crust. We suggest that the sealed horizon was extended to breaking point during the 1982–84 crisis, caused by the intrusion of

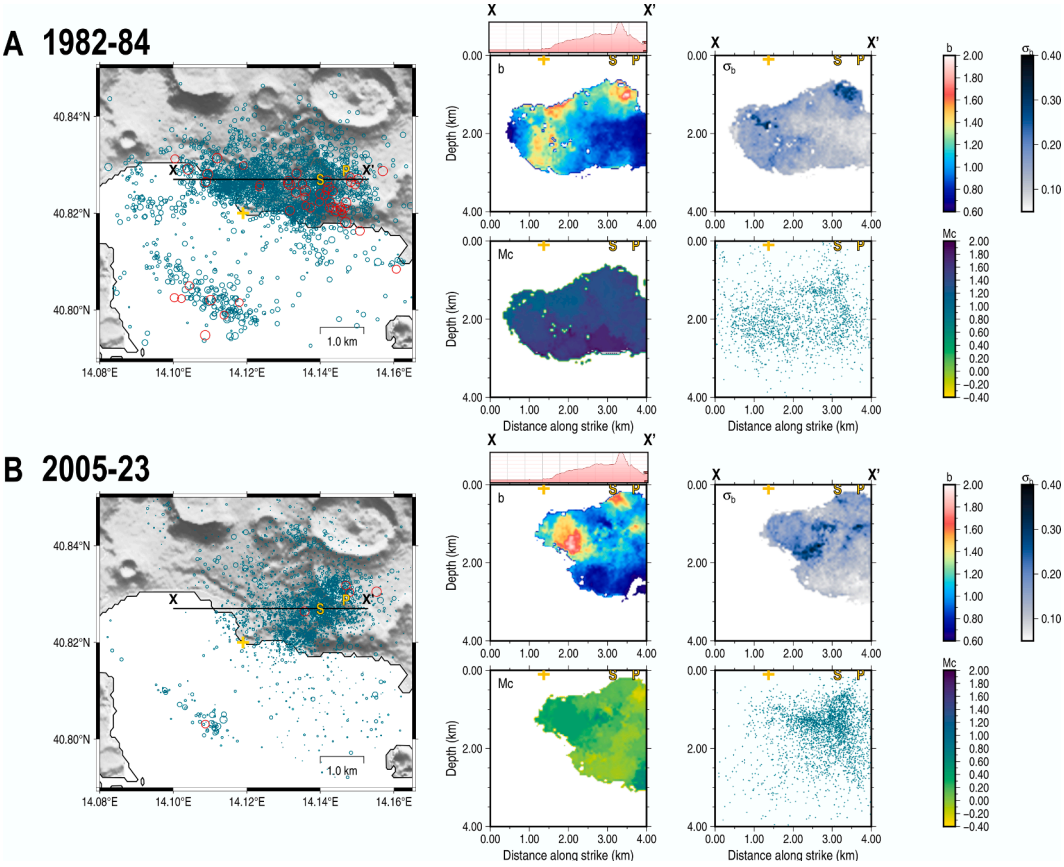

Fig. 8. Maps of earthquake relative locations (green circles) of earthquakes for 1982–84 (A) and 2005–2023 (B); red circles are events with $M_d \geq 3$. In both cases, XX' is the EW-oriented profile used for the vertical sections. The vertical sections represent the distribution of the Gutenberg-Richter *b*-value calculated in a volume 2 km wide around XX', the corresponding standard deviation σ_b, the magnitude of completeness M_c and the distribution of seismic locations projected on the vertical section. The topographic elevation along the profile XX' is obtained from Google Earth Pro. Pozzuoli, Solfatara and Pisciarelli are marked in yellow.

magma and its release of additional magmatic gas below the BDTZ. Before the seismic swarm of April 1st, 1984, by which time Pozzuoli had been raised by about 150 cm (Fig. 4D), the rate of uplift had been increasing (Fig. 4D) and most of the seismicity had occurred in a volume of c. 4–5 km^3 of the crust above the BDTZ (Figs 7 and 4Sa). After the swarm, the rate of uplift began to decline (Fig. 4D), the number of earthquakes with magnitude $M_d \geq 3$ increased towards Solfatara (Figs. 2 and 3) and the proportion of CO_2 increased in the gases escaping from Solfatara (Chiodini et al., 2012). All three changes are consistent with the swarm breaching the BDTZ, allowing magmatic fluids and pressurised gases to escape into the overlying crust (Fig. 3S).

Magmatic gas that had accumulated in the pressure source escaped towards Solfatara, increasing the rate of CO_2 emission and, by reducing the source pressure, initiated the decline in the rate of uplift (Fig. 4). The increase in the number of $M_d \geq 3$ earthquakes would have also been favoured by a combination of perturbations in the shallow stress field at the time of the swarm and an increase in pore pressure from the gases migrating towards Solfatara. Depressurization due to a net loss in gas also explains the subsidence at the CFc between 1984 and 2004 (Todesco, 2021; Kilburn et al., 2023).

The seismically active segment above the BDTZ in 1982–84 has not shown the same diffuse seismicity during the uplift since 2005, suggesting that some of the previous breaches were successfully resealed during the preceding subsidence. Resealing would also favour a return to slow uplift, when gases from magma 7–9 km underground were able to replenish the shallow source (Kilburn et al., 2023). Fig. 7 shows the thickness of the seismogenic crust using the depth of the 90 % cut-off (D90) as a practical measure of the BDTZ (Supplementary Material). The shapes of the D90 levels in 1982–84 and 2005–23 are remarkably similar and both become thicker away from the central area of the caldera between Pozzuoli and Solfatara (Fig. 7). However, the present depth of 2.2 ± 0.1 km for the D90 boundary beneath Solfatara is less than its 2.6 ± 0.1 km in 1982–84. The difference may reflect local heating, and potential weakening, of the crust as a result of an increased supply of steam and magmatic gas (Chiodini et al., 2021), although, this remains a qualitative interpretation. In contrast, the D90 boundary beneath Pozzuoli appears deeper today than it was in 1982–84. This suggests that it has not been similarly heated by gas flow, which is consistent with the BDTZ beneath Pozzuoli having become a sealed horizon.

4.3. *Focussed gas escape through Solfatara-Pisciarelli*

Resealing of the BDTZ across the central part of the caldera has focussed degassing beneath Solfatara. The concentration of low-magnitude seismicity below the eastern end of the cap rock (Figs 5 and 6) suggests that the accumulation of magmatic gas unable to escape through Solfatara has been a major control on the amount of local fracturing below Solfatara-Pisciarelli fumaroles. Seismicity at the Solfatara end of the cap rock has also been characterised by *b*-values of between 1.4 and 2.0, more than twice the background values of 0.8–0.9, both before breaching in 1982–84 and after resealing by 2005 (Fig. 8). High *b*-values, greater than those observed for purely tectonic event frequency-magnitude distributions (Mogi, 1962; Warren and Latham, 1970), are promoted by local increases in pore pressure. Independent evidence for high local pore pressures is provided by seismic tomography, which has recorded anomalously high values for seismic P-wave velocity, as well as high values for the ratio of P- to S- wave velocities

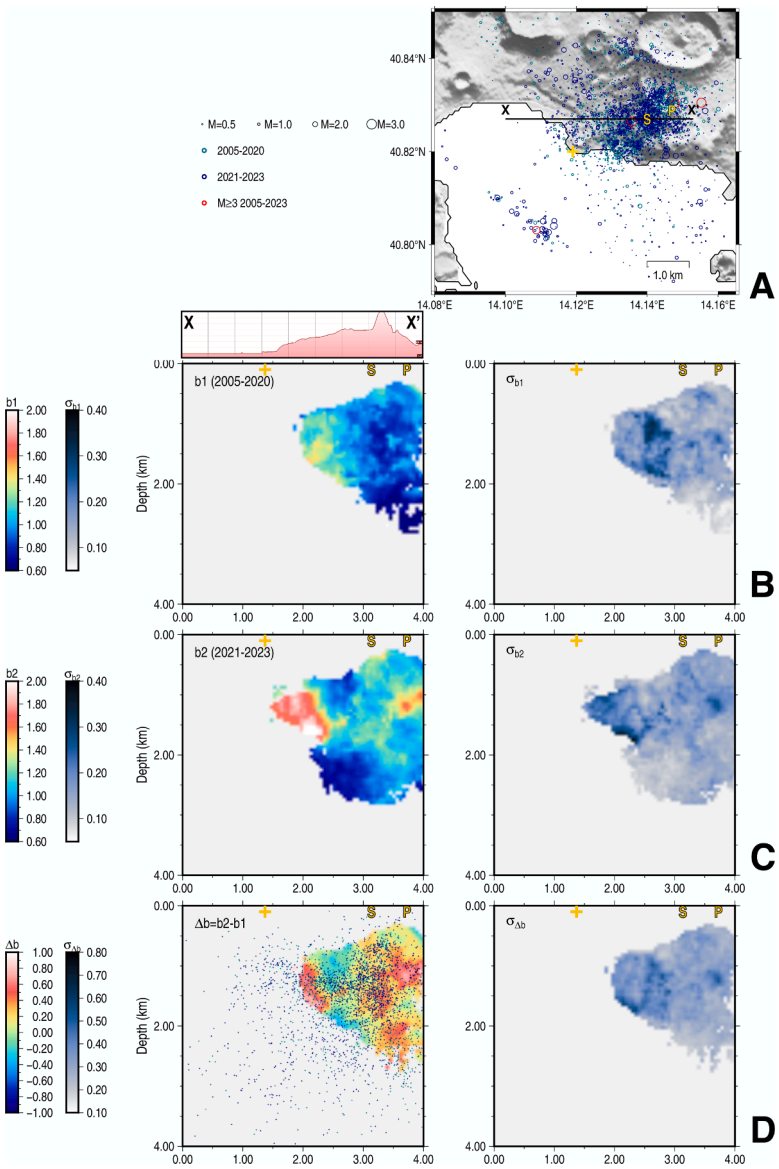

Fig. 9. Variation of the *b*-value during 2005–2020 and 2021–2023. (A) Map of earthquake relative locations (green and blue circles, code colour in legend) for the years 2005–2023. XX' is a EW-oriented profile used for the definition of vertical sections. (B) The vertical sections represent the distribution of the Gutenberg-Richter b-value for 2005–2020 (b1) calculated in a volume 2 km wide around XX' and the corresponding standard deviation σ_{b1}. The topographic elevation along the profile XX' is obtained from Google Earth Pro. (C) As for B for 2021–2023 (b2). (D) The difference $\Delta b = b_2 - b_1$ and corresponding standard deviation $\sigma_{\Delta b}$. The distribution of seismicity in 2005–2023 (blue points) is superimposed on Δb. Pozzuoli, Solfatara and Pisciarelli are marked in yellow.

below Solfatara (Fig. 5S; Calò and Tramelli, 2018). The *b*-value below Solfatara-Pisciarelli has been gradually increasing since 2021 by about 70–80% (Fig. 9). By extension of our arguments for Solfatara, we attribute the increase to the accumulation of magmatic gas beneath the whole of the deforming crust. Analogy with *b*-value data from compressional failure (Scholz, 2015) may also indicate a decrease in the applied differential stress.

4.4. Future scenarios

In addition to the increasing rates of low-magnitude seismicity, 14 earthquakes with magnitudes M_d of 3 or more have occurred since 2019 - all at depths between 2 and 3.5 km and with epicentres about 2.0–2.5 km away from the centre of uplift (beyond Solfatara and Pisciarelli to the NE and along an offshore fault to the SW; Fig. 6). They are the first earthquakes of such magnitude to have been recorded during the post-2005 uplift. Their late onset (compared to the beginning of unrest) and hypocentral positions suggest that the slip along larger faults has been caused by the bending of the crust exceeding a critical amount. One exception to the distribution is the magnitude 3.6 earthquake that occurred on 11 June 2023 along the western edge of La Starza at a depth of 2.7 km. The location lies at the western edge of the 1982–84 seismogenic zone and close to the BDTZ.

The pressure source driving unrest at CFc lies beneath the geothermal system. Its location suggests that the BDTZ is strong, as well as impermeable, and acts as a natural barrier to the ascent of fluids, whether magma or magmatic gas. Rupture and resealing of the BDTZ have thus modulated ground movement and seismicity by controlling the flow of magmatic fluids from below the geothermal system (Fig. 10). Uplift since 2005 has again extended the crust, bringing the BDTZ closer to conditions favourable to renewed rupture and enhanced surface degassing (Kilburn et al., 2023). Potential outcomes depend on where rupture occurs and how abruptly it changes the flow of gas. Assuming a pattern of rupture similar to that in 1984, scenarios range from a slowing

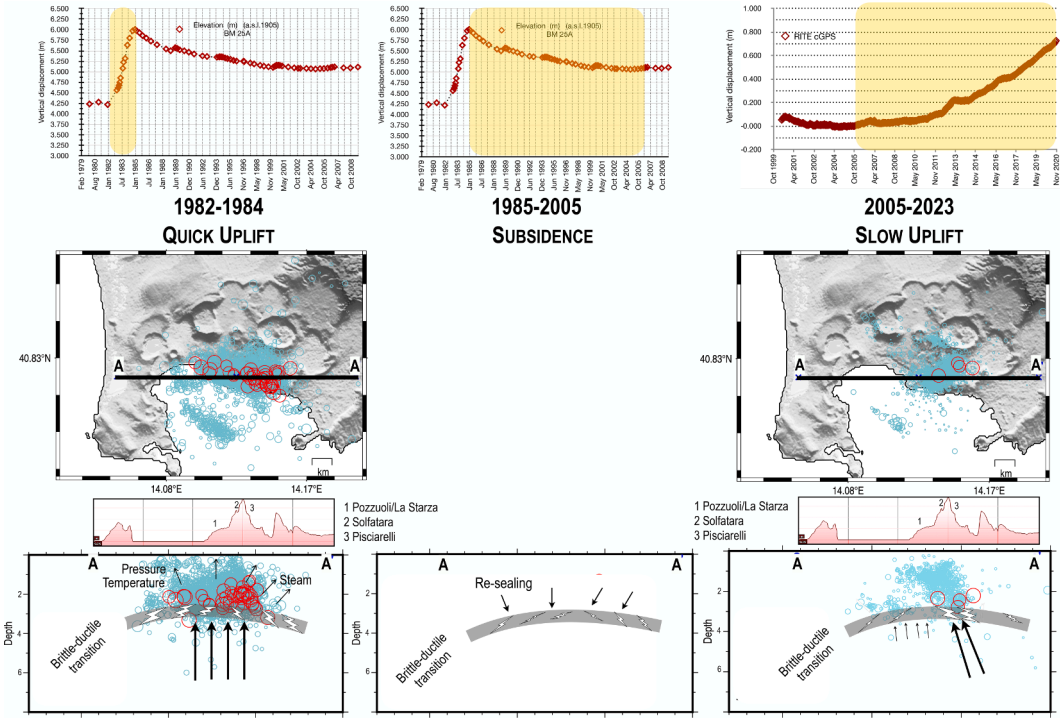

Fig. 10. Conceptual model of unrest at CFc since 1982. (Top) The sequence of ground vertical deformation in 1982–84, 1985–2005 and 2005–2021 obtained from levelling measurements at benchmark Bm25A (Pozzuoli) and at the cGPS station RITE (De Martino et al., 2021). (Middle) The corresponding relative locations of earthquakes (blue). Events with $M_d \geq 3$ are shown in red. (Bottom) Vertical sections with relocated seismicity projected along the EW profile (AA') and cartoon of the state of fracturing across the BDTZ as suggested by seismicity.

of uplift, either to rest or to a renewed subsidence, to a geothermal explosion of gas and vaporised groundwater in the vicinity of Solfatara-Pisciarelli. However, the emergence of seismicity near the BDTZ away from Solfatara (Fig. 8) raises the possibility of enhanced gas release from parts of the caldera not affected by such surface activity during recent episodes of unrest.

An implicit assumption in these scenarios is that conditions have not changed significantly for releasing gas from the parent magmatic system 7–9 km below the surface. In this case, changes in gas flux can be related to changes in fluid pressure between the deep source (assumed constant) and the BDTZ (which changes with the rate of gas escape to the surface; Kilburn et al., 2023). An alternative to be tested is that new magma arriving from depths greater than 9 km has pressurized the parent system, increasing its rate of gas release and so favouring both a faster rate of accumulation at the level of the BDTZ and continued surface uplift. In this case, the change in gas flux may reflect the approach to conditions suitable for renewed magma ascent and either a shallow intrusion and episode of rapid uplift, as in 1982–84 or, if the magma reaches the new rupture, a magmatic eruption.

5. Conclusions

Since 1982, seismicity and strain energy release at Campi Flegrei have been concentrated between two low-permeability horizons at depths of about 1.5 and 3 km, respectively. The horizons are natural controls on the circulation of fluids within the volcano's geothermal system. The deeper horizon coincides with a Brittle-Ductile Transition Zone (BDTZ) along the base of the system: above the base, pore pressures are hydrostatic and the crust behaves in an elastic-brittle manner; below the base, pore pressures can reach lithostatic values and deformation is mostly aseismic. The shallower low-permeability horizon marks a cap rock that separates the circulation of near-surface fluids from the flow of fluids within the deeper levels of the geothermal system.

Ground movements have been controlled by pressure changes below the BDTZ. Uplift occurs when new fluids enter the crust that is already rich in CO_2. The new fluids may be magma, gas released from that magma, or an increased discharge of gas from depth. They stretch the overlying crust until the BDTZ is ruptured. In 1982–84, the rapid uplift starting in June-July 1982 began to decay after the seismic swarm of April 1st, 1984. Nine months later, ground uplift had halted, to be followed by slow subsidence until 2004–05 and then the slow uplift that is still continuing (November 2023).

The sequence is consistent with rapid uplift during the intrusion of magma and release of its gas. The seismic swarm in April 1984 ruptured the BDTZ and allowed gas to escape. The rate of degassing increased from Solfatara-Pisciarelli and reduced pressure in the source region. Continued gas escape promoted subsidence until the BDTZ had resealed itself sufficiently to again trap gas arriving from depth and to initiate slow uplift at a rate comparable to (but in the opposite direction of) that during the preceding uplift (Fig. 10). Resealing has also focused gas flow towards Solfatara-Pisciarelli, raising local pore pressures and thermal gradient and favouring the concentration of seismicity in the adjacent eastern section of the Starza fault (Figs. 7 and 8).

Should the ongoing uplift continue (November 2023), a new episode of rupturing can be expected across the BDTZ. Potential outcomes range from a reversal of ground movement, in the least dangerous scenario, to geothermal explosions or possibly even a magmatic eruption, in the most catastrophic scenario, if new magma were to reach the uppermost layers of the crust. Our results thus provide a foundation for integrating additional geophysical and geochemical monitoring data, as well as surface observations, to identify the likelihood of each scenario and when it might occur.

Funding

SD, NAP and SC were funded by the BEST CaFE Project, under the INGV Working Earth Project, supported by the Ministry of University and Research.

CRediT authorship contribution statement

Stefania Danesi: Writing – review & editing, Writing – original draft, Visualization, Formal analysis, Conceptualization. **Nicola Alessandro Pino:** Writing – review & editing, Supervision, Project administration, Methodology, Conceptualization. **Stefano Carlino:** Writing – review & editing. **Christopher R.J. Kilburn:** Writing – review & editing.

Declaration of Competing Interest

The authors declare that the research was conducted in the absence of any commercial or financial relationships that could be construed as a potential conflict of interest.

Data availability

Data are publicly available through INGV's dedicated web services.

Acknowledgments

We are grateful to two anonymous reviewers for their constructive comments and valuable suggestions, which have greatly improved the quality of the manuscript. We thank Patrizia Ricciolino ("Laboratorio di Sismologia" INGV Naples) for providing us with the arrival times of the seismic phases. Maps and vertical sections are created using the Free and Open Source QGIS (2022) and GMT6 (Wessel et al., 2019). Some plots and data analysis are made with Rstudio (2022).

Supplementary materials

Supplementary material associated with this article can be found, in the online version, at doi:10.1016/j.epsl.2023.118530.

References

Akande, W.G., Gan, Q., Cornwell, D.G., Siena, L.D., 2021. Thermo-hydro-mechanical model and cap rock deformation explain the onset of an ongoing seismo-volcanic unrest. J. Geophys. Res. Solid Earth 126. https://doi.org/10.1029/2020jb020449.

Aster, R.C., Meyer, R.P., 1988. Three-dimensional velocity structure and hypocenter distribution in the Campi Flegrei caldera, Italy. Tectonoph 149 (3–4), 195–218. https://doi.org/10.1016/0040-1951(88)90173-4.

Barberi, F., Corrado, G., Innocenti, F., Luongo, G., 1984. Phlegraean Fields 1982–1984: brief chronicle of a volcano emergency in a densely populated area. Bull. Volcanol. 47, 175–185. https://doi.org/10.1007/bf01961547.

Bellucci, F., Woo, J., Kilburn, C.R.J., Rolandi, G., 2006. Ground deformation at Campi Flegrei, Italy: implications for hazard assessment. Geol. Soc. Lond. Spec. Publ. 269, 141–157. https://doi.org/10.1144/gsl.sp.2006.269.01.09.

Benioff, H., 1951. Earthquakes and Rock Creep. BSSA, pp. 31–62.

Berrino, G., 1994. Gravity changes induced by height-mass variations at the Campi Flegrei caldera. J. Volcanol. Geoth. Res. 61, 293–309. https://doi.org/10.1016/0377-0273(94)90010-8.

Bianco, F., Caliro, S., Martino, P.D., Orazi, M., Ricco, C., Vilardo, G., et al., 2022. Campi Flegrei, A restless caldera in a densely populated area. Act. Volcanoes World 219–237. https://doi.org/10.1007/978-3-642-37060-1_8.

Bonafede, M., Amoruso, A., Crescentini, L., Gottsmann, J.H., Todesco, M., Trasatti, E., 2022. Campi Flegrei, a restless caldera in a densely populated area. Active Volcanoes World 283–309. https://doi.org/10.1007/978-3-642-37060-1_11.

Buono, G., Paonita, A., Pappalardo, L., Caliro, S., Tramelli, A., Chiodini, G., 2022. New insights into the recent magma dynamics under campi flegrei caldera (Italy) from petrological and geochemical evidence. J. Geophys. Res. Solid Earth 127. https://doi.org/10.1029/2021jb023773.

Buono, G., Caliro, S., Paonita, A., Pappalardo, L., Chiodini, G., 2023. Discriminating carbon dioxide sources during volcanic unrest: the case of Campi Flegrei caldera (Italy). Geology. https://doi.org/10.1130/g50624.1.

Caliro, S., Chiodini, G., Moretti, R., Avino, R., Granieri, D., Russo, M., Fiebig, J., 2007. The origin of the fumaroles of La Solfatara (Campi Flegrei, South Italy). Geochim. Cosmochim. Acta 71, 3040–3055. https://doi.org/10.1016/j.gca.2007.04.007.

Caliro, S., Chiodini, G., Paonita, A., 2014. Geochemical evidences of magma dynamics at Campi Flegrei (Italy). Geochim. Cosmochim. Acta 132, 1–15. https://doi.org/10.1016/j.gca.2014.01.021.

Calò, M., Tramelli, A., 2018. Anatomy of the Campi Flegrei caldera using enhanced seismic tomography models. Sci. Rep.-uk 8, 16254. https://doi.org/10.1038/s41598-018-34456-x.

Carlino, S., 2018. Heat flow and geothermal gradients of the Campania region (Southern Italy) and their relationship to volcanism and tectonics. J. Volcanol. Geoth. Res. 365, 23–37. https://doi.org/10.1016/j.jvolgeores.2018.10.015.

Castaldo, R., D'Auria, L., Pepe, S., Solaro, G., Novellis, V.D., Tizzani, P., 2019. The impact of crustal rheology on natural seismicity: campi Flegrei caldera case study. Geosci. Front. 10, 453–466. https://doi.org/10.1016/j.gsf.2018.02.003.

Chiodini, G., Caliro, S., De Martino, P., Avino, R., Gherardi, F., 2012. Early signals of new volcanic unrest at Campi Flegrei caldera? Insights from geochemical data and physical simulations. Geology 40, 943–946. https://doi.org/10.1130/g33251.1.

Chiodini, G., Caliro, S., Avino, R., Bini, G., Giudicepietro, F., Cesare, W.D., Ricciolino, P., Aiuppa, A., Cardellini, C., Petrillo, Z., Selva, J., Siniscalchi, A., Tripaldi, S., 2021. Hydrothermal pressure-temperature control on CO2 emissions and seismicity at Campi Flegrei (Italy). J. Volcanol. Geoth. Res. 107245 https://doi.org/10.1016/j.jvolgeores.2021.107245.

Corrado, G., Guerra, I., Bascio, A.L., Luongo, G., Rampoldi, R., 1977. Inflation and microearthquake activity of phlegraean fields, Italy. Bull. Volcanol. 40, 169–188. https://doi.org/10.1007/bf02596998.

Cusano, P., Petrosino, S., Saccorotti, G., 2008. Hydrothermal origin for sustained Long-Period (LP) activity at Campi Flegrei Volcanic Complex, Italy. J. Volcanol. Geotherm. Res. 177, 1035–1044. https://doi.org/10.1016/j.jvolgeores.2008.07.019.

D'Auria, L., Giudicepietro, F., Aquino, I., Borriello, G., Gaudio, C.D., Bascio, D.L., Martini, M., Ricciardi, G.P., Ricciolino, P., Ricco, C., 2011. Repeated fluid-transfer episodes as a mechanism for the recent dynamics of Campi Flegrei caldera (1989–2010). J. Geophys. Res. Solid Earth 116. https://doi.org/10.1029/2010jb007837, 1978 2012.

D'Auria, L., Pepe, S., Castaldo, R., Giudicepietro, F., Macedonio, G., Ricciolino, P., Tizzani, P., Casu, F., Lanari, R., Manzo, M., Martini, M., Sansosti, E., Zinno, I., 2015. Magma injection beneath the urban area of Naples: a new mechanism for the 2012–2013 volcanic unrest at Campi Flegrei caldera. Sci. Rep. 5, 13100. https://doi.org/10.1038/srep13100.

De Martino, P., Dolce, M., Brandi, G., Scarpato, G., Tammaro, U., 2021. The ground deformation history of the Neapolitan Volcanic Area (Campi Flegrei Caldera, Somma–Vesuvius Volcano, and Ischia Island) from 20 years of continuous GPS observations (2000–2019). Remote Sens.-Basel 13, 2725. https://doi.org/10.3390/rs13142725.

De Siena, L., Amoruso, A., Pezzo, E.D., Wakeford, Z., Castellano, M., Crescentini, L., 2017. Space-weighted seismic attenuation mapping of the aseismic source of Campi Flegrei 1983–1984 unrest. Geophys. Res. Lett. 44, 1740–1748. https://doi.org/10.1002/2017 gl072507.

De Vivo, B., Rolandi, G., 2020. Volcanological risk associated with Vesuvius and Campi Flegrei. Chapter in Vesuvius, Campi Flegrei, and Campanian Volcanism, pp. 471–493. https://doi.org/10.1016/B978-0-12-816454-9.00017-1.

Del Gaudio, C., Aquino, I., Ricciardi, G.P., Ricco, C., Scandone, R., 2010. Unrest episodes at Campi Flegrei: a reconstruction of vertical ground movements during 1905–2009. J. Volcanol. Geoth. Res. 195, 48–56. https://doi.org/10.1016/j.jvolgeores.2010.05.014.

Del Pezzo, E., De Natale, G., Martini, M., Zollo, A., 1987. Source parameters of microearthquakes at Phlegraean Fields (Southern Italy) volcanic area. Phys. Earth Planet In. 47, 25–42. https://doi.org/10.1016/0031-9201(87)90064-1.

Di Luccio, F., Pino, N.A., Piscini, A., Ventura, G., 2015. Significance of the 1982–2014 Campi Flegrei seismicity: preexisting structures, hydrothermal processes, and hazard assessment. Geophys. Res. Lett. 42, 7498–7506. https://doi.org/10.1002/2015GL064962.

Di Vito, M.A., Acocella, V., Aiello, G., Barra, D., Battaglia, M., Carandente, A., Del Gaudio, C., de Vita, S., Ricciardi, G.P., Ricco, C., Scandone, R., Terrasi, F., 2016. Magma transfer at Campi Flegrei caldera (Italy) before the 1538 AD eruption. Sci. Rep.-UK 6, 32245. https://doi.org/10.1038/srep32245.

Dvorak, J.J., Berrino, G., 1991. Recent ground movement and seismic activity in Campi Flegrei, southern Italy: episodic growth of a resurgent dome. J. Geophys. Res. Solid Earth 96, 2309–2323. https://doi.org/10.1029/90jb02225.

Dvorak, J.J., Mastrolorenzo, G., 1991. The mechanisms of recent vertical crustal movements in Campi Flegrei caldera, southern Italy. Geological Society of America. Springer. https://doi.org/10.1130/SPE263. ISBN 3540426426, 9783540426424.

Fournier, 1999. Hydrothermal processes related to movement of fluid from plastic into brittle rock in the magmatic-epithermal environment. Economic geology and the bulletin of the Society of Economic Geologists, Hydrothermal processes related to movement of fluid from plastic into brittle rock in the magmatic-epithermal environment 94, 1193–1212.

Global Volcanism Program, 1989. Report on Campi Flegrei (Italy) (McClelland, L., ed.). Scientific Event Alert Network Bulletin, 14:6. Smithsonian Institution. https://doi.org/10.5479/si.GVP.SEAN198906-211010 (accessed October 2023).

Gottsmann, J., Rymer, H., Berrino, G., 2006a. Unrest at the Campi Flegrei caldera (Italy): a critical evaluation of source parameters from geodetic data inversion. J. Volcanol. Geoth. Res. 150, 132–145. https://doi.org/10.1016/j.jvolgeores.2005.07.002.

Gottsmann, J., Folch, A., Rymer, H., 2006b. Unrest at Campi Flegrei: a contribution to the magmatic versus hydrothermal debate from inverse and finite element modeling. J. Geophys. Res.: Solid Earth 111 (B7). https://doi.org/10.1029/2005JB003745.

Gutenberg, B., Richter, C.F., 1955. Magnitude and energy of earthquakes. Nature 176, 795. https://doi.org/10.1038/176795a0.

INGV 2023, Surveillance Bulletins https://www.ov.ingv.it/index.php/monitoraggio-e-infrastrutture/bollettini-tutti/bollett-mensili-cf/anno-2023-1, in Italian.

Kanamori, H., 1977. The energy release in great earthquakes. J. Geophys. Res. 82, 2981–2987. https://doi.org/10.1029/jb082i020p02981.

Kilburn, C.R.J., Natale, G.D., Carlino, S., 2017. Progressive approach to eruption at Campi Flegrei caldera in southern Italy. Nat. Commun. 8, 15312. https://doi.org/10.1038/ncomms15312.

Kilburn, C.R.J., Carlino, S., Danesi, S., Pino, N.A., 2023. Potential for rupture before eruption at Campi Flegrei caldera, Southern Italy. Commun. Earth Environ. 4, 190. https://doi.org/10.1038/s43247-023-00842-1.

Klein, F.W., 2002. Open-File Report 2002-171. https://doi.org/10.3133/ofr02171.

Lima, A., Bodnar, R.J., Vivo, B.D., Spera, F.J., Belkin, H.E., 2021. Interpretation of Recent Unrest Events (Bradyseism) at Campi Flegrei, Napoli (Italy): Comparison of models based on cyclical hydrothermal events versus shallow magmatic intrusive events. Geofluids 2021, 1–16. https://doi.org/10.1155/2021/2000255.

Macedonio, G., Giudicepietro, F., D'Auria, L., Martini, M., 2014. Sill intrusion as a source mechanism of unrest at volcanic calderas. J. Geophys. Res.: Solid Earth 119, 3986–4000. https://doi.org/10.1002/2013jb010868.

Mogi, K., 1962. Study of elastic shocks caused by the fracture of heterogeneous materials and its relations to earthquake phenomena. Bull. Earthquake Res. Inst. Tokyo Univ. 40 (125), 196.

Natale, J., Camanni, G., Ferranti, L., Isaia, R., Sacchi, M., Spiess, V., Steinmann, L., Vitale, S., 2022. Fault systems in the offshore sector of the Campi Flegrei caldera (southern Italy): implications for nested caldera structure, resurgent dome, and volcano-tectonic evolution. J. Struct. Geol. 163, 104723 https://doi.org/10.1016/j.jsg.2022.104723.

Orsi, G., Civetta, L., Gaudio, C.D., Vita, S.de, Vito, M.A.D., Isaia, R., Petrazzuoli, S.M., Ricciardi, G.P., Ricco, C., 1999. Short-term ground deformations and seismicity in the resurgent Campi Flegrei caldera (Italy): an example of active block-resurgence in a densely populated area. J. Volcanol. Geoth. Res. 91, 415–451. https://doi.org/10.1016/s0377-0273(99)00050-5.

Petrosino, S., Siena, L.D., Pezzo, E.D., 2008. Recalibration of the Magnitude Scales at Campi Flegrei, Italy, on the basis of measured path and site and transfer functionsrecalibration of the magnitude scales at Campi Flegrei, Italy. B Seismol. Soc. Am. 98, 1964–1974. https://doi.org/10.1785/0120070131.

Petrosino, S., Siena, L.D., 2021. Fluid migrations and volcanic earthquakes from depolarized ambient noise. Nat. Commun. 12, 6656. https://doi.org/10.1038/s41467-021-26954-w.

QGIS Development Team, 2022. QGIS Geographic Information System. Open Source Geospatial Foundation Project. http://qgis.osgeo.org.

Ricciolino, P., Lo Bascio, D., 2021. Cataloghi sismici dei vulcani campani. Stazione STH Campi Flegrei dal 2000 al 2021 (CatSTH_2000_2021) (1.0) [Data set]. Istituto Nazionale di Geofisica e Vulcanologia (INGV). doi:10.13127/ovcatalogsth_2000_2021.

Rivalta, E., Corbi, F., Passarelli, L., Acocella, V., Davis, T., Vito, M.A.D., 2019. Stress inversions to forecast magma pathways and eruptive vent location. Sci. Adv. 5, eaau9784. https://doi.org/10.1126/sciadv.aau9784.

RStudio Team, 2022. RStudio: Integrated Development For R. RStudio. PBC. URL. http://www.rstudio.com/.

Scarpa, R., Bianco, F., Capuano, P., Castellano, M., D'Auria, L., Di Lieto, B., Romano, P., 2022. Historic Unrest of the Campi Flegrei Caldera, Italy. Campi Flegrei, A Restless Caldera in a Densely Populated Area. Active Volcanoes World. https://doi.org/10.1007/978-3-642-37060-1.

Scholz, C.H., 2015. On the stress dependence of the earthquake b value. Geophys. Res. Lett. 42, 1399–1402. https://doi.org/10.1002/2014 gl062863.

Suzuki, Z., 1959. A statistical study on the occurrence of small earthquakes (fourth paper). Sci. Rep. Tohoku Univ. Ser. 5 Geophysics 11 (1), 10–54.

Tamburello, G., Caliro, S., Chiodini, G., De Martino, P., Avino, R., Minopoli, C., Carandente, A., Rouwet, D., Aiuppa, A., Costa, A., Bitetto, M., Giudice, G., Francofonte, V., Ricci, T., Sciarra, A., Bagnato, E., Capecchiacci, F., 2019. Escalating CO2 degassing at the Pisciarelli fumarolic system, and implications for the ongoing Campi Flegrei unrest. J. Volcanol. Geoth. Res. 384, 151–157. https://doi.org/10.1016/j.jvolgeores.2019.07.005.

Todesco, M., 2021. Caldera's Breathing: poroelastic ground deformation at Campi Flegrei (Italy). Front. Earth Sci. 9, 702665 https://doi.org/10.3389/feart.2021.702665.

Tramelli, A., Godano, C., Ricciolino, P., Giudicepietro, F., Caliro, S., Orazi, M., et al., 2021. Statistics of seismicity to investigate the Campi Flegrei caldera unrest. Sci. Rep.-UK 11, 7211. https://doi.org/10.1038/s41598-021-86506-6.

Tramelli, A., 2022. Seismic catalogue Campi Flegrei 1982-1984 [Data set]. Zenodo. https://doi.org/10.5281/zenodo.6810718.

Troise, C., De Natale, G., Schiavone, R., Somma, R., Moretti, R., 2019. The Campi Flegrei caldera unrest: discriminating magma intrusions from hydrothermal effects and implications for possible evolution. Earth-Sci. Rev. 188, 108–122. https://doi.org/10.1016/j.earscirev.2018.11.007.

Vanorio, T., Kanitpanyacharoen, W., 2015. Rock physics of fibrous rocks akin to Roman concrete explains uplifts at Campi Flegrei Caldera. Science 349, 617–621. https://doi.org/10.1126/science.aab1292.

Waldhauser, F., 2001. HypoDD: a computer program to compute double-difference earthquake locations. USGS Open File Rep. 01–113.

Warren, N.W., Latham, G.V., 1970. An experimental study of thermally induced microfracturing and its relation to volcanic seismicity. J. Geophys. Res. 75, 4455–4464. https://doi.org/10.1029/jb075i023p04455.

Wessel, P., Luis, J.F., Uieda, L., Scharroo, R., Wobbe, F., Smith, W.H.F., Tian, D., 2019. The generic mapping tools version 6. Geochem. Geophys. Geosyst. 20, 5556–5564. https://doi.org/10.1029/2019GC008515.

White, R., McCausland, W., 2016. Volcano-tectonic earthquakes: a new tool for estimating intrusive volumes and forecasting eruptions. J. Volcanol. Geotherm. Res. 309, 139–155. https://doi.org/10.1016/j.jvolgeores.2015.10.020.

Wiemer, S., Wyss, M., 2000. Minimum magnitude of completeness in earthquake catalogs: examples from Alaska, the Western United States, and Japan. B. Seismol. Soc. Am. 90, 859–869. https://doi.org/10.1785/0119990114.

Woo, J.Y.L., Kilburn, C.R.J., 2010. Intrusion and deformation at Campi Flegrei, southern Italy: sills, dikes, and regional extension. J. Geophys. Res. Solid Earth 115. https://doi.org/10.1029/2009jb006913, 1978 2012.